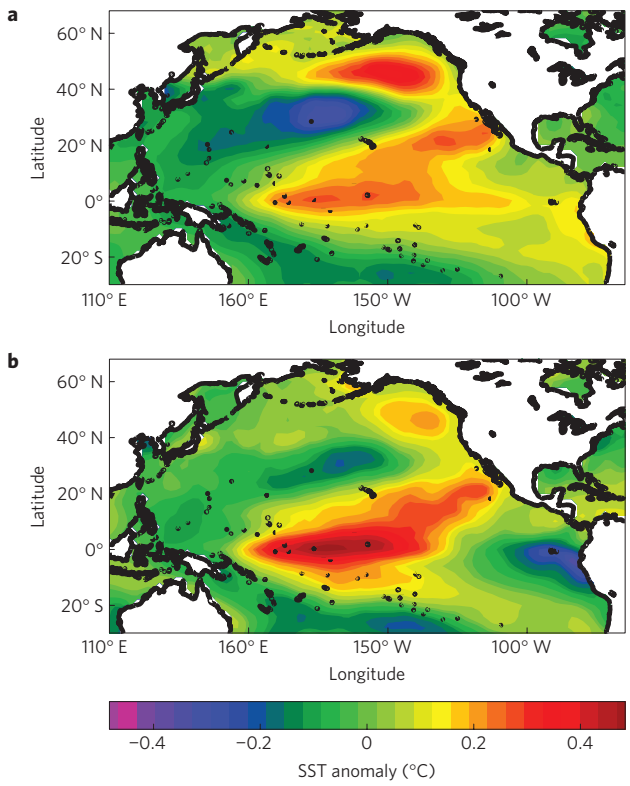

Figure 1 | Spatial structure of SST anomalies of the CPW El Niño and the NPGO. a,**b**, The NPGO (**a**) and the CPW (**b**) patterns are obtained by regressing the monthly NOAA SST anomaly reanalysis with the CPW and NPGO indices, respectively.

Previous studies have linked the NPGO's atmospheric forcing pattern (Fig. 2a) to intrinsic variability associated with the North Pacific Oscillation[10] (NPO; Supplementary Fig. S1). The NPO, defined as the second dominant mode of SLP variability in the North Pacific[20], is also characterized by two centres of action, one over Alaska and another north of Hawaii, and is widely regarded as a purely stochastically driven phenomenon intrinsic to the North Pacific atmosphere[20]. However, analyses of Pacific SLP fields indicate that the low-frequency (>8 yr) variability of the NPO (Supplementary Fig. S1) also bears a strong resemblance to the CPW SLP pattern, including strong low-frequency variance in the Hawaiian region (158° W–135° W; 13° N–24° N). This comparison is consistent with the hypothesis that low-frequency variations of SLP in the Hawaii region, which are an important contributor to the NPGO's low-frequency variability, are linked to SST anomalies in the central tropical Pacific associated with CPW.

Results from atmospheric general circulation model (AGCM) simulations coupled to a mixed-layer ocean model (ML) lend further support to the idea that the low-frequency variations of the atmospheric SLP over the Hawaiian region, here measured with the SLP_{HI} index, are driven by changes in central tropical Pacific SSTs. We use a 45-member ensemble of the AGCM–ML (ref. 21; see the Methods section), wherein each ensemble member is forced with prescribed SST anomalies from 1950 to 2008 in a narrow region in the equatorial Pacific (12° S–12° N), and interactive fluxes between the AGCM and the ML elsewhere. We isolate the specific tropical SST pattern that drives the deterministic component of the model's resulting SLP_{HI} variability by correlating, for each AGCM–ML ensemble member, the model's SLP_{HI} values during boreal winter (January–February–March, JFM)—the period in which the SLP_{HI} variance is maximum—with the corresponding JFM tropical Pacific SST anomalies that force each simulation. The average correlation map that emerges from the 45-member ensemble reveals a significant correlation pattern in the tropical Pacific (maximum $R = 0.65$; >99%; Fig. 3a). The maximum positive correlations are located in the central tropical Pacific between 220° W and 150° W, which is a defining characteristic of the JFM SST anomaly pattern associated with the CPW (Fig. 3b). The link to the CPW is also evident from the significant correlation between the CPW index and the AGCM–ML SLP_{HI} ensemble mean ($R = 0.6$; >99%; Fig. 3c). It is important to note that the AGCM–ML atmospheric ensemble members have no feedback onto tropical Pacific SST

Figure 2 | The atmospheric forcing of the NPGO. a, Correlation of the NPGO index with monthly NCEP SLP anomalies. The SLP anomalies averaged over the white rectangle east of Hawaii are used to derive an index of the atmospheric forcing of the NPGO, referred to as the SLP_{HI} index. **b**, Correlation map of the CPW index with NCEP SLP anomalies. **c**, The NPGO index (blue) is reconstructed (black) using an AR1 model forced by the SLP_{HI} index. The units are in standard deviations (s.d.). The significance of correlation ($R = 0.65$; >99%) of the raw monthly values is estimated using a Monte Carlo test for time series with a corresponding red spectra (see the Methods section).

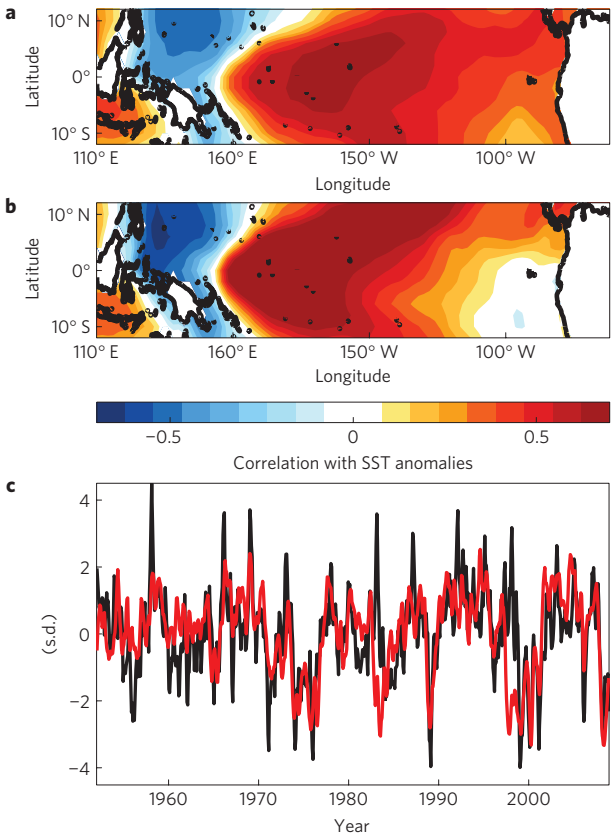

Figure 3 | Tropical Pacific SST anomaly forcing pattern for the AGCM–ML SLP_{HI}. **a**, Ensemble average correlation map of the AGCM–ML SLP_{HI} index with SST anomalies in the tropical Pacific (12° S–12° N) during winter time (JFM). The correlation is computed separately for each AGCM–ML realization of the SLP_{HI} and then all correlation maps are averaged together so that the average correlation retains both the signal and noise of the AGCM–ML. **b**, The correlation pattern of the CPW index with SST anomalies during winter (JFM). **c**, Time series of the AGCM–ML SLP_{HI} ensemble mean (black) and the CPW index (red). Indices are normalized by their standard deviations and are correlated $R = 0.6$ (>99%). The significance of correlation of the raw monthly values is estimated using a Monte Carlo test for time series with a corresponding red spectra (see the Methods section).

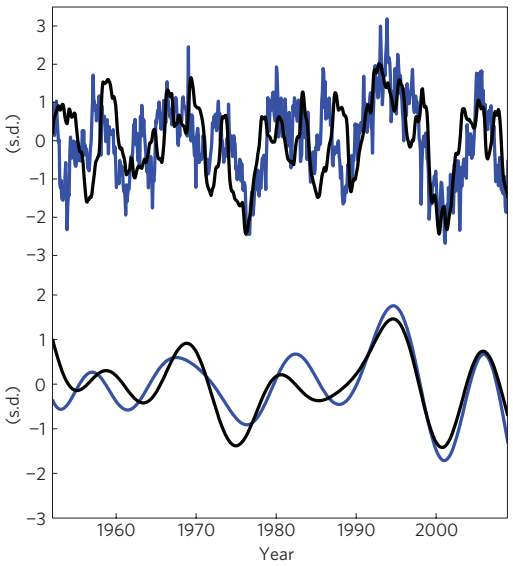

Figure 4 | Reconstruction of NPGO variance originating from the tropical Pacific. The NPGO index (blue) is reconstructed (black) by forcing an AR1 model with the time series of the AGCM–ML SLP_{HI} ensemble mean, which represent the deterministic variability driven by the central tropical Pacific. The units are in standard deviations (s.d.). The significance of correlation of the raw monthly (top panel) ($R = 0.55$; >99%; top) and 8-year low-pass-filtered (bottom panel) ($R = 0.85$; >98%; bottom) values is estimated using a Monte Carlo test for time series with red spectra (see the Methods section).

anomalies; therefore, the significant correlations observed between the modelled SLP_{HI} index and the tropical Pacific SST indicate a one-way forcing from the tropical Pacific to the extratropics. These correlations suggest that >25% of the SLP_{HI} variability is forced by CPW and imply that the low-frequency variability of SLP_{HI}, and by extension the NPO, is forced by tropical SST variability.

To quantify how much of the NPGO variance is driven by the tropically forced component of the SLP_{HI} we apply the AR1 model introduced above to each of the 45 model-derived SLP_{HI} indices (see also the Methods section). The ensemble mean reconstruction of the NPGO index is significantly correlated with the original NPGO index[4] ($R = 0.55$, >99%; Fig. 4). The correlations between the modelled and original NPGO indices are maximized on low-frequency (>8 yr) timescales (Fig. 4; $R = 0.85$; >99%). The low-frequency character of the modelled NPGO indices is a direct result of tropical SST forcing—if we remove the ensemble mean SLP_{HI} from each ensemble member, thereby removing that component of tropically forced response common to all of the AGCM–ML SLP_{HI} time series, we find that the individual ensemble members' reconstructed NPGO indices are uncorrelated to the original NPGO index ($R = 0.04$). Therefore, we conclude that the forced component of SLP_{HI} variability that drives the NPGO originates from SST anomalies in the equatorial Pacific.

Taken together, our results suggest that the low-frequency character of the NPGO, an important source of ocean climate and ecosystem variability in the Pacific, originates from coupled ocean–atmosphere interactions associated with the CPW phenomenon. The NPGO–CPW dynamical link proposed here echoes that previously identified to explain the relationship between the PDO and ENSO. Several studies have linked the midlatitude variability of the PDO to the canonical expression of ENSO, both statistically and dynamically[12–14,22,23]. The dynamics that link ENSO to PDO are referred to as the 'atmospheric bridge'[12], whereby atmospheric teleconnections to the extratropics excited by ENSO project onto the atmospheric variability of the Aleutian Low, which then drives the ocean PDO pattern. Employing the same modelling approach used to isolate the 'atmospheric bridge', this study demonstrates that a similar dynamical chain is triggered by central tropical Pacific SST anomalies (CPW or Modoki El Niño). CPW drives changes in the large-scale atmospheric circulation in the central North Pacific (for example, NPO), which are then integrated by the ocean to yield the NPGO. Whereas the impacts of the PDO on Pacific marine ecosystems and North American climate patterns are extensively documented[1], the impacts of the newly discovered NPGO across the Pacific Basin are just beginning to emerge[4,9–11,15,24].

These findings imply that a large fraction of low-frequency climate variability in the North Pacific is driven by tropical Pacific climate variability. Therefore, large uncertainties of the tropical Pacific's response to climate change[25] may limit the predictability of future changes in Pacific decadal-scale climate. However, if climate model projections suggesting an increase in the frequency of CPW under anthropogenic global warming scenarios are accurate[8], then NPGO variance may also increase. Consistent with this view, NPGO variability has intensified in the late twentieth century[4], explaining a growing number of late-twentieth-century climate and ecosystem indices across the North Pacific basin[4,9–11,15,24]. As an

important indicator of physical (for example, strength of gyre-scale circulation, eastern-boundary upwelling) and biological (nutrients, chlorophyll *a*, fish species) fluctuations in the North Pacific at both the coastal and basin scales, an increase in NPGO power would have broad implications. This is especially true for marine ecosystems, which amplify decadal-scale environmental fluctuations into strong state transitions and therefore may exhibit a high sensitivity to ongoing climate change.

Methods

The observational analyses use monthly anomalies of SLP from the National Centers for Environmental Protection (NCEP) Reanalysis II[26] and SST from the National Oceanic and Atmospheric Administration (NOAA) Reanalysis[27]. The monthly anomalies are computed by removing the climatological monthly means.

The CPW index and pattern are defined by computing the first principal component of tropical SST anomalies between 20° S and 20° N after removing the canonical ENSO using regression of the SST variability associated with the Nino3 index (http://www.cpc.noaa.gov/data/indices).

The NPGO index[21] (http://www.o3d.org/npgo) is defined as the second principal component of sea surface height anomalies in the northeast Pacific (180°–110° W; 25° N–62° N) and was originally obtained from an ocean model hindcast[4] forced by the NCEP Reanalysis II[26] surface fluxes. This method of computing the NPGO index is valid to the extent that the NPGO is predominantly an ocean response to large-scale atmospheric forcing over the North Pacific, as suggested by previous studies[10]. We confirmed this finding with an independent estimate of the NPGO index from the Japanese Earth Simulator global eddy-resolving ocean model[28] (OFES). The OFES model hindcast was also forced by the NCEP fluxes and its monthly NPGO index shares >70% of variance ($R = 0.86$) with the original NPGO index[4]. This shared variance can be interpreted as one estimate of the amount of NPGO variance that is forced by the atmosphere. We also quantified the sensitivity of the NPGO atmospheric forcing pattern by comparing the patterns that emerge from the NCEP SLP Reanalysis (Fig. 2a) and Hadley SLP2 Reanalysis[29]. These forcing patterns were computed by correlating the NPGO index with the SLP anomalies of the NCEP and Hadley data sets. We find that these SLP patterns are significantly correlated ($R = 0.98$).

The oceanic NPGO response to atmospheric forcing is quantified using an autoregressive model of order 1 (AR1),

$$\frac{\mathrm{dNPGO_{rec}}(t)}{\mathrm{d}t} = \mathrm{SLP_{HI}}(t) - \frac{\mathrm{NPGO_{rec}}(t)}{\tau_{\mathrm{NPGO}}}$$

where the rate of change of the NPGO index is forced by the $\mathrm{SLP_{HI}}$, defined as the time series of average NCEP SLP anomalies over the Hawaiian region (158° W–135° W; 13° N–24° N; Fig. 2a, white rectangle). The $\mathrm{SLP_{HI}}$ is here used as an index of the atmospheric forcing of the NPGO. The ocean memory to the $\mathrm{SLP_{HI}}$ perturbations is represented in the damping term (second term on the right-hand side). The timescale of the damping τ_{NPGO} is computed from the decorrelation timescale of the NPGO index (~10 months), consistent with previous studies[10]. We also forced the AR1 model with the Hadley SLP2 data[29] to quantify whether errors in the NCEP reanalysis could affect our ability to reconstruct the NPGO. We found that the NCEP and Hadley NPGO reconstructions are essentially identical, with correlations of 0.96, with only minor discrepancies in the early 1950s.

The significance of the correlation coefficients is estimated from the probability distribution functions of the correlation coefficient of two red-noise time series with the same autoregression coefficients as estimated from the original signals. The probability distribution functions are computed numerically by generating 3,000 realizations of the correlation coefficient of two random red-noise time series.

The AGCM–ML simulations are carried out using the International Center for Theoretical Physics atmospheric general circulation model coupled to an ocean mixed-layer of 50 m fixed depth[21]. This model was selected on the basis of its ability to capture the observed large-scale atmospheric variability and tropical teleconnection as demonstrated within the Climate of the 20th Century CLIVAR project[21].

Received 2 April 2010; accepted 17 September 2010; published online 17 October 2010

References

1. Hare, S. R. *et al.* Inverse production regimes: Alaska and West Coast Pacific salmon. *Fisheries* **24,** 6–14 (2000).
2. Mantua, N., Hare, S., Zhang, Y., Wallace, J. & Francis, R. A Pacific interdecadal climate oscillation with impacts on salmon production. *Bull. Am. Meteorol. Soc.* **78,** 1069–1079 (1997).
3. Martinez, E., Antoine, D., D'Ortenzio, F. & Gentili, B. Climate-driven basin-scale decadal oscillations of oceanic phytoplankton. *Science* **326,** 1253–1256 (2009).
4. Di Lorenzo, E. *et al.* North Pacific Gyre Oscillation links ocean climate and ecosystem change. *Geophys. Res. Lett.* **35,** L08607 (2008).
5. Larkin, N. & Harrison, D. Global seasonal temperature and precipitation anomalies during El Niño autumn and winter. *Geophys. Res. Lett.* **32,** L16705 (2005).
6. Ashok, K. & Yamagata, T. Climate change: The El Niño with a difference. *Nature* **461,** 481–484 (2009).
7. Kug, J., Jin, F. & An, S. Two types of El Niño Events: Cold tongue El Niño and warm pool El Niño. *J. Clim.* **22,** 1499–1515 (2009).
8. Yeh, S-W. *et al.* El Niño in a changing climate. *Nature* **461,** 511-U70 (2009).
9. Di Lorenzo, E. *et al.* Nutrient and salinity decadal variations in the central and eastern North Pacific. *Geophys. Res. Lett.* **36,** L14601 (2009).
10. Chhak, K. C., Di Lorenzo, E., Schneider, N. & Cummins, P. F. Forcing of low-frequency ocean variability in the northeast Pacific. *J. Clim.* **22,** 1255–1276 (2009).
11. Ceballos, L. I., Di Lorenzo, E., Hoyos, C. D., Schneider, N. & Taguchi, B. North Pacific gyre oscillation synchronizes climate fluctuations in the eastern and western boundary systems. *J. Clim.* **22,** 5163–5174 (2009).
12. Alexander, M. *et al.* The atmospheric bridge: The influence of ENSO teleconnections on air–sea interaction over the global oceans. *J. Clim.* **15,** 2205–2231 (2002).
13. Vimont, D. The contribution of the interannual ENSO cycle to the spatial pattern of decadal ENSO-like variability. *J. Clim.* **18,** 2080–2092 (2005).
14. Newman, M., Compo, G. & Alexander, M. ENSO-forced variability of the Pacific decadal oscillation. *J. Clim.* **16,** 3853–3857 (2003).
15. Sydeman, W. J. & Thompson, M. A. *The California Current Integrated Ecosystem Assessment (IEA), Module II: Trends and Variability in Climate-Ecosystem State.* Report to NOAA/NMFS/Environmental Research Division (2010).
16. Kim, H., Webster, P. & Curry, J. Impact of shifting patterns of Pacific Ocean warming on north Atlantic tropical cyclones, **325** 77–80 (2009).
17. Weng, H., Behera, S. K. & Yamagata, T. Anomalous winter climate conditions in the Pacific rim during recent El Niño Modoki and El Niño events. *Clim. Dyn.* **32,** 663–674 (2009).
18. Hoerling, M. & Kumar, A. Atmospheric response patterns associated with tropical forcing. *J. Clim.* **15,** 2184–2203 (2002).
19. Frankignoul, C. & Hasselmann, K. Stochastic climate models. Part II: Application to sea surface temperature anomalies and thermocline variability. *Tellus* **29,** 289–305 (1977).
20. Rogers, J. The North Pacific Oscillation. *J. Climatol.* **1,** 39–57 (1981).
21. Bracco, A., Kucharski, F., Kallummal, R. & Molteni, F. Internal variability, external forcing and climate trends in multi-decadal AGCM ensembles. *Clim. Dyn.* **23,** 659–678 (2004).
22. Pierce, D., Barnett, T. & Latif, M. Connections between the Pacific Ocean tropics and midlatitudes on decadal timescales. *J. Clim.* **13,** 1173–1194 (2000).
23. Deser, C., Phillips, A. & Hurrell, J. Pacific interdecadal climate variability: Linkages between the tropics and the North Pacific during boreal winter since 1900. *J. Clim.* **17,** 3109–3124 (2004).
24. Menge, B. M., Chan, F., Nielsen, K. J., Di Lorenzo, E. & Lubchenco, J. Climatic variation alters supply-side ecology: Impact of climate patterns on phytoplankton and mussel recruitment. *Ecol. Monogr.* **79,** 379–395 (2009).
25. Collins, M. *et al.* The impact of global warming on the tropical Pacific ocean and El Niño. *Nature Geosci.* **3,** 391–397 (2010).
26. Kalnay, E. *et al.* The NCEP/NCAR 40-year reanalysis project. *Bull. Am. Meteorol. Soc.* **77,** 437–471 (1996).
27. Smith, T. M. & Reynolds, R. Improved extended reconstruction of SST (1854–1997). *J. Clim.* **17,** 2466–2477 (2004).
28. Sasaki, H. *et al.* in *High Resolution Numerical Modelling of the Atmosphere and Ocean* (eds Hamilton, K. & Ohfuchi, W.) Ch. 10, 157–186 (Springer, 2008).
29. Allan, R. & Ansell, T. A new globally complete monthly historical gridded mean sea level pressure dataset (HadSLP2): 1850–2004. *J. Clim.* **19,** 5816–5842 (2006).

Acknowledgements

We acknowledge the support of the NSF OCE-0550266, GLOBEC-0606575, OCE-0452654, OCE-0452692, CCS-LTER, GLOBEC OCE-0815280, OCE05-50233, NASA NNG05GC98G, Office of Science (BER), DOE DE-FG02-07ER64469 and JAMSTEC.

Author contributions

E.D.L. and N.S. carried out the analysis. E.D.L., K.M.C., N.S. and B.A. contributed to the writing of the paper. A.B. and J.C.F. contributed to the coupled ocean–atmosphere model. M.A.A. and D.V. contributed to the experimental design and analysis of the atmospheric teleconnection patterns. All authors discussed and commented on the layout and the results of the manuscript.

Additional information

The authors declare no competing financial interests. Supplementary information accompanies this paper on www.nature.com/naturegeoscience. Reprints and permissions information is available online at http://npg.nature.com/reprintsandpermissions. Correspondence and requests for materials should be addressed to E.D.L.